Band-moment Compression of AVIRIS Hyperspectral Data and its Use in the Detection of Vegetation Stress

L. Estep* and B. Davis**

* Lockheed Martin Space Operations - Stennis Programs, Bldg. 1210, Stennis Space Center, MS 39529

Phone: 228-688-7354, FAX: 228-688-3636, e-mail: lestep@ssc.nasa.gov

** NASA, Bldg. 1100, Stennis Space Center, MS 39529

Phone: 228-688-1921, FAX: 228-688-3636, e-mail: bdavis@ssc.nasa.gov

Earth Science Applications Directorate

Abstract

A remote sensing campaign was conducted over a U.S. Department of Agriculture test farm at Shelton, Nebraska. An experimental field was set off in plots that were differentially treated with anhydrous ammonia. Four replicates of 0-kg/ha to 200-kg/ha plots, in 50-kg/ha increments, were set out in a random block design. Low-altitude (GSD of 3 m) Airborne Visible/Infrared Imaging Spectrometer (AVIRIS) hyperspectral data was collected over the site in 224 bands. Simultaneously, ground data was collected to support the airborne imagery. In an effort to reduce data load while maintaining or enhancing algorithm performance for vegetation stress detection, band-moment compression and analysis was applied to the AVIRIS image cube. The results indicate that band-moment techniques compress the AVIRIS dataset significantly while retaining the capability of detecting environmentally induced vegetation stress.

Potential Applications/Areas

Data Compression, Earth Remote Sensing, Anomaly Detection

1.0 Introduction

The objective of this research was to employ band-moment compression of an Airborne Visible/Infrared Imaging Spectrometer (AVIRIS) hyperspectral image cube while retaining an ability to detect crop stress with the resulting imagery. In particular, nutrient stress detection is of primary importance. Nutrient stress is often a chief consideration when variation in plant pigmentation is observed (Schepers et al. 1996; Maas and Dunlap, 1989).

The relevant test site was the U.S. Department of Agriculture's (USDA's) Shelton, Nebraska, Variable Rate (VRAT) Nitrogen Application farm. This farm represents a historically well-documented corn growing quarter section. The USDA VRAT site is used to systematically study nutrient stress in corn by varying inter-plot application of fertilizer. The field has four replicates of five plots, which vary by nitrogen treatment from 0-kg/ha to 200-kg/ha in 50-kg/ha increments. The treatment plots are set out in a randomized, complete plot design.

Typically, the VRAT is planted in a ridge till, monoculture corn and is watered by a central pivot irrigation system that is on a three-day cycle. Since water stress can increase spectral reflectance from corn leaves (Wooley, 1971), it is important that the field be adequately watered so that only nutrient-related stress will predominate. Figure 1 shows imagery of the USDA VRAT site with the fertilizer amounts for each plot shown.

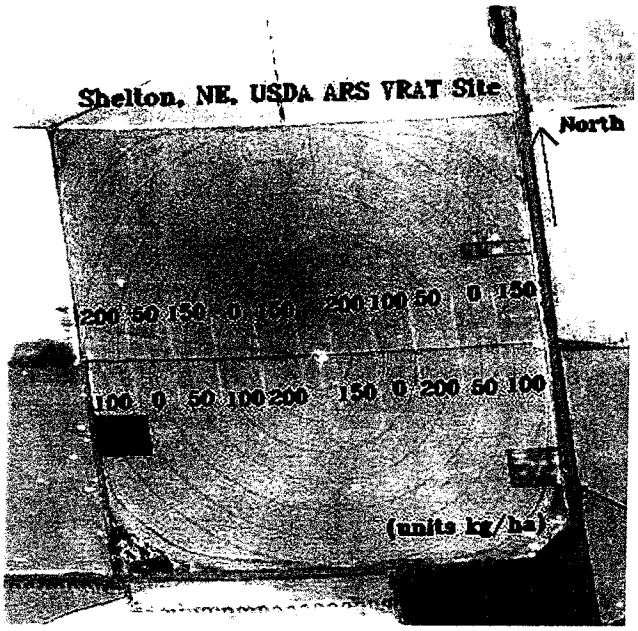

Figure 1. ATLAS near-infrared image of USDA VRAT study site.

Low-altitude AVIRIS hyperspectral imagery was acquired over the Shelton, Nebraska, VRAT site on July 22, 1999. The overflight produced 3 m pixels with 224 spectral bands. Ground personnel supported the mission with measurements at the time of the overflight.

The Atmosphere Removal (ATREM) Program (Gao et al., 1992) was used to perform an atmospheric correction on the data. The AVIRIS imagery after ATREM correction is output as relative reflectance. This relative reflectance file was scaled by an empirical line procedure to provide reflectances that matched closely those measured in the field.

1.1 Spectral Band Considerations

Using AVIRIS image data from the MAC Europe 1991 campaign, Clevers (1999) determined that the 224 bands of spectral information over agricultural sites could be compressed significantly by performing a principal component analysis (PCA) on the data. Clevers (1999) determined that 3 factors explained 96.8% of the total variance in the dataset. The

first factor comprised a broad spectral band in the near-infrared (NIR) region that ranges from about 730 nm to 1350 nm. The second factor comprised two distinct spectral regions. The first region is in the visible region from about 500 nm to 700 nm, and the second region is in the short-wave infrared (SWIR) region that runs from 1500 nm onwards. The third factor is associated with a few bands around the red-edge region, or around 717 nm.

Thenkabail et al. (2000) has recommended a set of hyperspectral bands for agricultural studies. The total spectral range of the 12 bands described run from about 495 nm to 1025 nm. For each of the 12 band sets, a description of associated physical mechanisms that are involved for each specific spectral range is included.

In comparing the work by Clevers (1999) and Thenkabail et al. (2000), their spectral band sets, as might be expected, overlap. The bands 1 through 4 recommended by Thenkabail describe the green peak region. The bands 5 through 8 cover the red-edge region. Therefore, Clevers' second factor involves the first eight bands suggested by Thenkabail. Similarly, Clevers' first factor involves the final four band sets recommended by Thenkabail. These final four band sets are associated with the heightened "plateau" reflectance past the red-edge rise (Thenkabail's bands 9 and 10) and with water-sensitive bands (Thenkabail's bands 11 and 12).

The SWIR region, which Thenkabail et al. (2000) does not consider, is found to be significant in Clevers' analysis. Interestingly, Kokaly (2000) has shown leaf nitrogen concentration is assessable because of an absorption-broadening feature in the SWIR. Apparently, this is associated with plant protein amide bonds. Furthermore, the SWIR region is known to provide some sensitivity to certain soil characteristics, including relative soil and plant leaf moisture (Goetz and Boardman, 1995).

In this study, the band sets alluded to above -- namely, the green peak, the red-edge, the water sensitive bands, the NIR region, and the SWIR of Clevers (1999) -- will be considered. Furthermore, the entire Clevers band set and the less expansive band set of Thenkabail et al. (2000) will also be included. Table 1 provides a summary of these band set spectral ranges.

BAND SET NAMES	BAND SET SPECTRAL RANGES (NM)
Green peak	490 - 570
Red-edge	660 - 720
NIR	810 - 925
Water Sensitive	980 - 1000
SWIR	1500 - 2250
Clevers Total Band Set	117 bands (500 - 2250 nm)
Thenkabail et al. (2000)	12 bands (490 - 1025 nm)

Table 1. Band sets used in present study.

2.0 Band Moment Methodology Background

Image compression has acquired enhanced importance with the advent and availability of high spatial resolution multispectral imagery as well as the prospect of further hyperspectral, and even ultraspectral, advanced sensors on the horizon. The immediate goal of any image compression technique is to represent image data in the smallest number of bits. This allows an increase in processing speed and minimizes storage constraints. Both of these outcomes are especially important if fast turnaround of remotely sensed image data to product form is required to satisfy customer needs.

Compression, or coding, of an image can be either lossy or lossless. Lossless coding of an image would imply that no data is lost from the original image in the compression process. When

a compression technique is lossy, some of the image detail is permanently lost in the transformation to a compressed dataset.

The use of band-moments to characterize spectral imagery represents a form of lossy compression. The loss of information is a trade-off between information entropy and increased efficiency. If compression efficiency were defined in spectral terms, then the spectral compression efficiency might be defined as the simple ratio of the number of input sensor bands to the number of output bands provided by the compression algorithm. For instance, by generating eight band-moments to statistically characterize an AVIRIS image cube, a spectral compression efficiency of 224/8, or 28 to 1, is achieved.

A band-moments approach to hyperspectral image coding has been reported in the literature (Rundquist and Di, 1989; Staenz, 1996). Following these authors, eight (8) moments were computed. The germane moments are the following: 1) the ordinary moment, 2) the mean, 3) the second central moment (standard deviation), 4) the third central moment, 5) the fourth central moment, 6) band skewness, 7) band kurtosis, and 8) the band concentrated moment. In the aforementioned studies and the present one, band-moment compression of hyperspectral imagery has shown robustness with very little coding delay and is, of course, scalable. Additionally, Rundquist and Di (1989) found that the use of band-moment compression reduced sensor noise and, in their case, improved image quality.

Foundationally, Papoulis (1965) has shown that if the spectral reflectance is finitely non-zero and piecewise continuous, then statistical moments of any order exist and are unique. Hence, the band-moments associated with a set of spectral reflectances uniquely characterize that spectral dataset, and conversely (Rundquist and Di, 1989).

For the present work, a compressed spectral dataset will be evaluated for its crop stress detection capability by comparing relative outcomes between it and the original uncompressed spectral dataset from which it was derived.

It is interesting that an observer at the USDA VRAT field can visually detect the difference between the untreated and the 50-kg/ha plots and the controls, which are represented by 200-kg/ha plots. However, the 100- and 150-kg/ha plots are not readily differentiated from the controls by the human eye. This implies that, if relevant imagery can be processed so that this separation becomes possible, then pre-visual stress detection would have been attained. Pre-visual crop stress detection is a significant goal of crop stress research.

3.0 Approach

In this section, an overview of the analysis applied to the AVIRIS imagery will be given. In the next section, results generated from the analysis outlined here will be presented.

For a given band set from Table 1, AVIRIS imagery of the VRAT was used to extract region-of-interest (ROI) data from the different N-treatment plots. These extracted data were compiled and employed to compute eight band-moments, which in effect compressed the selected input band set (Table 1).

Compressed and uncompressed forms of the spectral band sets listed in Table 1 were used to compute the Euclidean and Bhattacharyya spectral class distances for the different N-treatment plots (the plots taken as classes). The spectral distances were used to determine whether the compressed band-moment band sets provided comparable separation of the VRAT N-treatment plot classes when compared to the original non-compressed band sets.

The spectral band sets of Table 1 were then ranked in order of those providing the greatest relative, spectral class (N-treatment plot) distances -- considering only the band-moment band sets -- for both the Euclidean and Bhattacharyya results. Then the eight moments associated with the top ranked band sets were plotted as box and whisker plots to determine which band moments appeared to show the greater sensitivity, or variation, as a function of N-treatment. The resulting band moments could then be compared to those previously determined by Staenz (1996). He performed a somewhat similar analysis upon a European agricultural dataset.

Band moments that proved more sensitive than others for a given Table 1 band set were used as single band images, in transformations, or in band ratios to produce imagery for the detection of crop stress. Possible band ratio forms paralleled those already known for use in the detection of plant stress. Such ratio forms might include versions of the Ratio Vegetation Index (RVI) (Jordan, 1969), Normalized Difference Vegetation Index (NDVI) (Rouse, 1973), Gitelson and Merzlyak (1996), or Schepers et al. (1996) algorithms. In the present study, the results for the Gitelson and Merzlyak (1996) and NDVI band ratio paradigms are provided.

A statistical comparison is made between uncompressed, AVIRIS hyperspectral band ratio imagery and the associated band-moment ratio imagery. Statistical testing using ANOVA methods and follow-on Dunnett multiple comparison tests are used to determine whether the band-moment, compressed band ratio imagery retains a separation of the N-treatment plots from the controls when compared to the uncompressed, hyperspectral band ratio imagery.

Supervised classification methods are exercised upon the uncompressed AVIRIS band sets of Table 1 and their associated band-moment band sets independently. A Figure-of-Merit comparison is made on the resulting classification images to assay the effects on crop stress detection by the lossy band-moment compression method.

4.0 Results and Discussion

The spectral distance results between the N-treatment plots (classes) for the Euclidean and Bhattacharyya distance measures were interesting. The Euclidean distance measure considers only the distance between class means and does not account for the potential overlap of classes (Thomas et al., 1987). The Bhattacharyya distance includes consideration of the spread, or variance/covariance, between the different class statistics in the computation of relative class separability.

The Euclidean distance computation results showed that the band-moment bands provided increased interclass separation compared to the original bands themselves for all the spectral band sets considered (Table 1). However, when Bhattacharyya distances were computed, the band-moment band sets fared less well. The spectral distance between classes for the band-moment bands only bettered the class separability of an uncompressed AVIRIS band set from Table 1 if the total number of bands of the original band set was equal to, or less than, the fixed eight bands that composed the band-moment band set.

The ranking outcome based upon the relative Bhattacharyya spectral distances (magnitudes) between the N-treatment plots for the band-moment band sets of Table 1 are as follows: 1) red-edge, 2) SWIR, 3) green peak, 4) NIR, and 5) water-sensitive bands of Thenkabail. If the compressed forms of the complete band sets suggested by Clevers (1999) and Thenkabail et al. (2000) are considered as well, then the spectral distance rankings would place them first and second, respectively, with the other band sets following as listed.

The individual band moments for the above top-ranked band sets were plotted as box-and-whisker plots, as a function of the N-treatment plots, for all spectral classes considered in Table 1. Succinctly, it was found that the band-moments that showed greatest sensitivity, in

order, were the third central moment, the first moment (ordinary moment), and the eighth moment (band concentrated moment) -- either singly or in combination. These results corroborate the findings of Staenz (1996).

4.1 Single Moment Imagery for Vegetative Stress Detection

Given the sensitivity of these particular moments, especially that of the third central moment, images displaying this computational result are interesting taken by themselves. Figure 2 exhibits the third central moment of the mean for the green peak spectral band set of Table 1. The third central moment is related to the skewness of a distribution. The equation for the skewness in this context is given by Equation (1):

$$skewness = \frac{\sum_{i=1}^{N} (Y_i - Y_{avg})^3}{(N-1)s^3} \qquad (1)$$

Since Figure 2 is computed pixel-by-pixel over the scene, it provides an approximate measure of the relative departure from a symmetrical distribution for the spectral brightness values that compose each pixel. The greater the departure, the darker the pixel. This is due to the chloritic nature of the more stressed regions in the field. The chlorosis causes a greater color variation than that seen in the more uniform, better nourished plots. This variation translates as an increased standard deviation, s. Since from Equation (1) above the skewness in normalized to s, the greater the variance, the smaller the value of the skewness -- hence, the darker the pixel.

It is interesting to note that the untreated VRAT plots exhibit the highest departure compared to the other plots present. In fact, it would appear that, in general, crop stress could be

associated with heightened asymmetry in the spectral distributions of the pixels that image a stressed crop region.

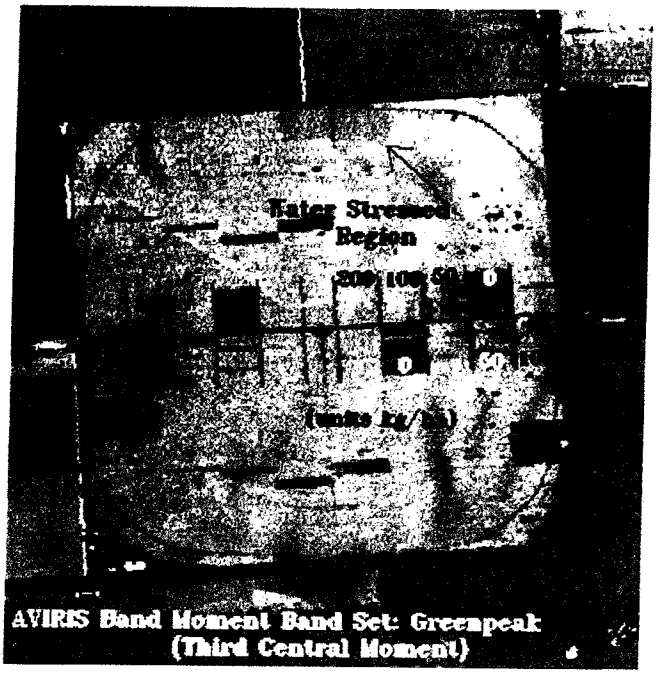

Figure 2. Third central moment green peak band set image of VRAT field.

As seen, Figure 2 shows considerable detail over the VRAT field. Broadly speaking, there are two sorts of stress registered by the image. The first is the nutrient stress in the different N-treatment plots. The second source of stress is water stress evidenced by a dark-toned band at the north-central periphery (top and central portion) of the field. The dark-toned band is an area that is deliberately water stressed by shutting off the central pivot irrigator as it passes over this section of the field. The presence of this water-stressed region can aid in attempting to separate one type of stress from the other. For example, Figure 3 shows the VRAT field in the eighth moment image (band concentrated mean) for the water-sensitive band set of Thenkabail et al. (2000).

Figure 3. Eighth moment of water-sensitive band set.

The clarity with which only the water-stressed region is displayed as a dark-toned area, while the nutrient-stressed areas associated with the N-treatment plots are comparatively muted or displayed as brighter areas, suggests a possible methodology for separating these two types of crop stress.

4.2 Band Moment Transformed or Used in Combination as Vegetation Indices

Different statistical moments for the different spectral band sets in Table 1 could be used in combination. That is, different transformations or ratio formulations could be employed using the band-moments band set of the compressed spectral image data. If the moments represent statistical summaries of various aspects of the distribution of spectral brightness over several bands, then the proposed indices may benefit from such aggregated measures. Of course, since

the moments represent statistical summaries over a range of spectral bands, they will emphasize some predominate trend of the spectral data. If the spread of the brightness values around the central tendency of the spectral data is large, then the ratios formed could be considered, in effect, broad bandwidth ratios -- even if the original image data represented hyperspectral bandwidths. Conversely, if the spread of the brightness values around the central tendency of the data clusters tightly around a specific wavelength, then the ratios would represent smaller bandwidth ratios -- ratios more akin to that of a hyperspectral dataset.

A principal component analysis could be run on the eight-band compressed, band-moment band set. Since the PCA analysis stacks the output imagery according to the amount of variance embedded in each image, with the image with greatest variance at the top of the output set, then the initial image exhibits as brightest those spectral features that provide the most variation in the scene. The next PCA image down in the output set is non-correlated with the first image and will highlight features that provide the next-most variation in the scene, and so forth. Embedded noise in the original imagery due to sensor and environmental sources increasingly appears as one proceeds through the stack of output PCA images, since noise, itself, provides a source of variation. The use of band-moment compression techniques serves to reduce the effects of noise, since the process is generally one of summation. Moreover, the noise present often tends to be Gaussian with mean near zero. So, when a band-moment band set is used as input to a PCA routine, the band output tends to show little or no effect from noise. Rather, the images move through a graded sequence of highlighting those image features that exhibit greater or lesser variation within the scene. Figure 4 displays an image that represents the third PCA band for an input green peak, eight-band, compressed dataset.

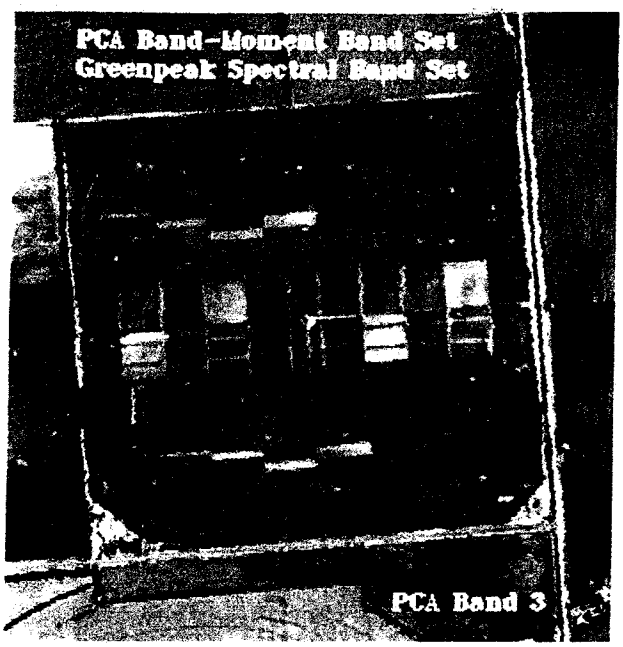

Figure 4. PCA band 3 of green-peak band-moment band set.

It is interesting that the image does not appear to show water stress effects. The stress exhibited is that due to the light-toned, nutrient-stress differences in the various plots. This PCA image represents a *de facto* separation of nutrient stress from water stress effects.

An example of a possible implementation of ratios is that of the third central moments of the green-peak and red-edge bands. This ratio emulates, to some extent, the ratio of bands suggested by Gitelson and Merzlyak (1996). Figure 5 displays the band-moment band set result of the Gitelson and Merzlyak ratio.

Figure 5. Third central moments of red-edge to green-peak ratio image.

As seen, Figure 5 provides considerable detail over the VRAT field. Certainly, the untreated N-treatment plots are clearly depicted. The gray tone scale provided within the image indicates a relative stress measure. Sensitivity to the water-stress region at the northern periphery of the VRAT field can be seen. Interestingly, the water-stressed area is a brighter region compared to the nutrient-stressed plot areas.

To assess whether the band-moment band set provides relatively reliable crop stress detection, a Gitelson-Merzlyak ratio image was computed using original, uncompressed AVIRIS hyperspectral bands. To provide a quantitative, head-to-head evaluation of these two Gitelson-Merzlyak images and their ability to separate the untreated, 50-, 100-, and 150-kg/ha plots from the controls (200-kg/ha), an ANOVA (Haber and Runyon, 1977) was run on plot data extracted

from these images. The data was extracted using ROI selections for each plot type and then compiling the result. In both cases, the ANOVA outcome allowed for the rejection of the null hypothesis at the $p < 0.0001$ level.

The follow-on Dunnett multiple comparisons test (Siegel, 1956) determined that the Gitelson and Merzlyak algorithm using the uncompressed AVIRIS bands could separate the 0-, 50-, and 100-kg/ha plots from the controls. The Dunnett multiple comparison for the compressed, band-moment ratio image documented that the very same plots could be distinguished from the controls. Hence, no loss of detection capability of vegetative stress occurred.

A normalized difference approach, such as that used by an NDVI algorithm, could also be implemented with selected band-moments. The NDVI algorithm aids in the removal of additive noise sources -- provided the wavelength regions associated with the band-moment in question have similar noise magnitudes. For example, if the eighth moments of the water-sensitive bands and the Clevers' SWIR region bands are input to an NDVI ratio, Figure 6 is the result.

Figure 6. Eighth moments of water-sensitive and SWIR band sets ratio image.

The image details crop stress but does not distinguish between nutrient stress and water stress. Note that since the linear irrigator is on a three-day cycle and moves anti-clockwise in the image, the area immediately in front of the movement of the irrigator shows signs of water stress, since it has been two days since it received water.

Whereas the NDVI algorithm (Rouse, 1973) endeavors to subtract out additive noise in the image data, ratio approaches, such as the RVI (Pearson and Miller, 1972), attempt to divide out multiplicative noise. Semenov and Yefremenko (1999) have suggested a form that allows for both additive and multiplicative noise removals. The form they provide is given as the following:

$$SALVI = \{(b1 - b2)\,(b2 - b3)\} / \max\{b1 - b2)^2\,, (b2 - b3)^2\} \qquad (2)$$

where "SALVI" stands for "Semenov Algorithm Vegetation Index" and b1, b2, and b3 are user-selected wavelengths.

The expression provided by Equation (2) is the form of a second moment of the brightness differences in the respective channels and resembles the computation of a cross-correlation coefficient for the respective bands. As can be seen, the expression will tend to remove multiplicative and additive noises from the selected channels, provided the relevant noise sources are roughly the same in all three channels.

Equation (2) was exercised with three band-moments as input bands. The band-moments employed were the third central moments of the red-edge, green-peak, and water-sensitive bands. For comparison, a similar computation using three analogous AVIRIS hyperspectral bands for the green-peak, red-edge, and water-sensitive regions was generated.

The SALVI image result yielded virtually the same appearance as in shown in Figure 5, with some slight differences. The SALVI image showed the water-stressed area as more clearly defined. Also, the bare-field areas on the west and east side of the VRAT field were shown containing, apparently, some vegetation. As it happens, for the July 22 AVIRIS overflight, some weed cover did, in fact, tarnish some portions of these bare-field regions. The comparable AVIRIS, original-band, SALVI-type image did not show this.

Using ANOVA methods and follow-up multiple comparison tests, it can be shown that both the compressed and uncompressed SALVI images can differentiate the untreated, 50-, and 100-kg/ha plots from the controls at approximately the same level of statistically accuracy. Thus, the use of three band moments in place of three analogous AVIRIS bands did not detract from stress-detection capability.

4.3 Supervised Classification Techniques and Class Discrimination

Using supervised classification techniques on both the band-moment band sets and the original band sets from which they were derived (Table 1), an attempt was made to separate the different N-treatment plots, or classes, from one another. Staenz (1996) used supervised classification techniques (maximum likelihood and logistic classifiers) on a band-moment band set to separate different field crops over a hyperspectral-imaged scene in Switzerland. His classification accuracy using the compressed hyperspectral image data was only slightly less than with the original hyperspectral image cube.

Figure 7 shows the result of applying the Spectral Angle Mapper (SAM) classifier algorithm to the compressed band-moment band set (8 bands) of the Clevers total band set referenced in Table 1. The SAM classifier was also applied to the uncompressed Clevers 117-band image. Since the earlier computed Bhattacharyya distances were much higher for Clevers' total band set, the expectation is that the larger band set, represented by Clevers' 117 bands, ought to allow enhanced class, or N-treatment plot, discrimination.

As can be seen, the image evinces varying degrees of stress, seen as an apparent fertilization application, over the VRAT field. The SAM application to Clevers' uncompressed band set image, using the full 117 bands, appeared virtually the same. Hence, although the Bhattacharyya distance computations for Clevers' original 117 bands are larger than those for the eight bands of the derived band-moment band set, the spectral class distances provided by the band-moment band set are apparently enough for the SAM classifier to provide satisfactory separation of the N-treatment plots.

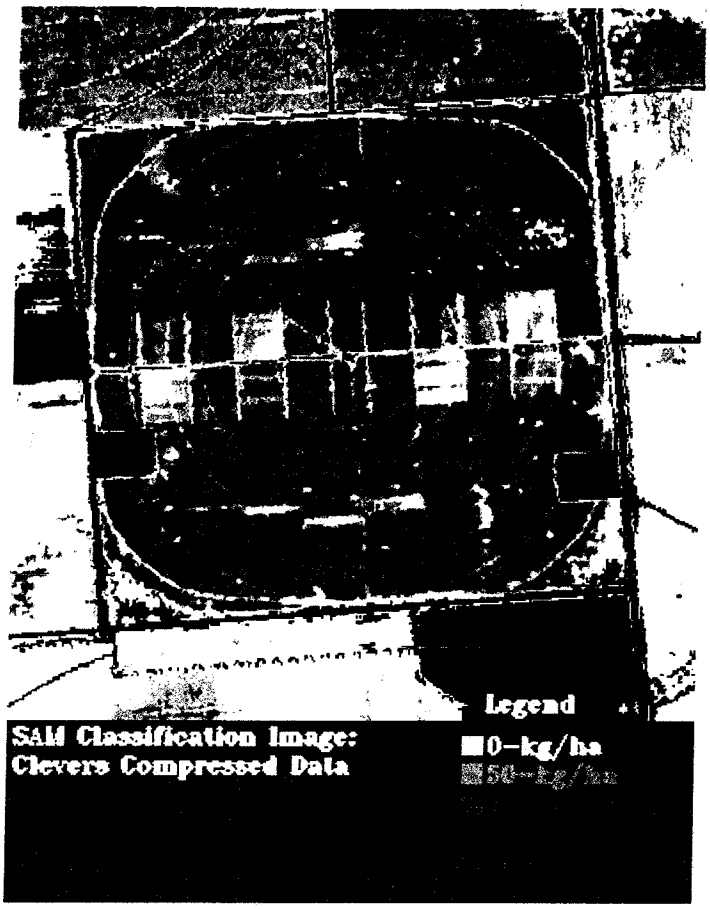

Figure 7. SAM classification image of Clevers' band-moment, or compressed, band set.

To show this quantitatively, averages and standard deviations of image data for the classified N-treatment plots were taken from both classification images. These mean and standard deviation values were scaled to an effective mean fertilizer application for each plot of the respective images. Figure 8 provide plots of these results (solid line represents the compressed image data).

Figure 7. SAM classification image of Clevers' band-moment, or compressed, band set.

To show this quantitatively, averages and standard deviations of image data for the classified N-treatment plots were taken from both classification images. These mean and standard deviation values were scaled to an effective mean fertilizer application for each plot of the respective images. Figure 8 provide plots of these results (solid line represents the compressed image data).

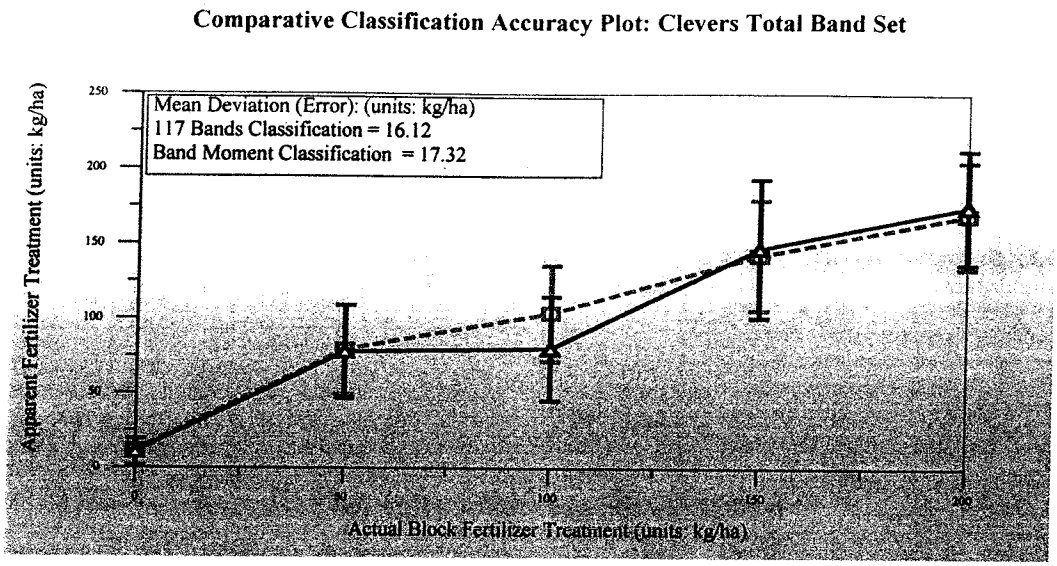

Figure 8. Figures of Merit for Clevers' total band set and associated band-moment band set.

As shown, the band-moment classification image, in terms of an apparent fertilizer application, compares favorably to the classification image that represents Clevers' total band set. The one principal offset is the 100-kg/ha plot value.

The mean deviation for all the points is computed and displayed on the graph for each plot separately. This provides an overall Figure of Merit on the relative quality of the classification accuracy.

The results, provided in Figure 8, corroborate Staenz's (1996) findings that a band-moment classification image has a somewhat lower classification accuracy when compared to an original band set classification image. Nonetheless, a gain is achieved in spectral compression, which translates into reduced storage requirements and shortened processing time for acquired imagery.

5.0 Summary and Conclusions

An AVIRIS image cube was subjected to compression using a band-moment methodology. Eight bands composed the compressed band set. These bands represent statistical moments that statistically summarize a given spectral band set.

The compressed and uncompressed band sets of Table 1 were compared to determine how the band-moment compression method affected the ability to detect crop stress (in corn) over a USDA test field. Since the band-moment compression procedure represents a lossy compression method, it was expected that some degradation of crop stress detection capability would occur.

The band-moment results derived from the compression process were analyzed in various ways. These band-moments were used as single band images for crop stress analysis, in transformation (PCA), and in ratio combinations to form novel vegetation indices.

The compressed band set was used as input to a standard SAM classification routine that generated a satisfactory classification image when compared to a similar classification image using the entire 117 bands of the original hyperspectral dataset.

In general, band-moment compression and analysis provides at least as good, or slightly less, capability for detecting crop stress than does the original band set from which it was derived. The benefit of the approach comes in increased noise immunity, decreased storage requirements, and increased speed of processing -- especially when dealing with multiple hyperspectral image cubes over extensive areas.

Acknowledgments

A portion of these data were kindly supplied by the USDA Agricultural Research Service, the Boeing Company, Batelle Pacific Northwest Research Laboratory, and University of California, Santa Barbara as part of a NASA-funded Earth Observations Commercial Applications Program project. This work was supported by the NASA Earth Science Applications Directorate under contract number NAS 13-650 at the John C. Stennis Space Center, Mississippi.

References

Clevers, J., 1999, The use of imaging spectrometry for agricultural applications. ISPRS Journal of Photogrammetry and Remote Sensing, 54: 299-304.

Gao, B. C., K. B. Heidebrecht, and A. F. H. Goetz, 1992, Atmospheric Removal Program (ATREM) User's Guide. Version 1.1, Center for the Study of Earth from Space document, University of Colorado, 24 p.

Gitelson, A. and M. Merzlyak, 1996, Signature analysis of leaf reflectance spectra: algorithm development for remote sensing of chlorophyll. J. Plant. Physiol., 148: 494-500.

Goetz, A. and J. Boardman, 1995, Spectroscopic measurement of leaf water status. Geoscience and Remote Sensing Symposium, IGARRS '95, Vol. 2: 978-980.

Haber, A. and R. Runyon, 1977, General Statistics. Addison-Wesley, Reading, MA.

Pearson, R. and L. Miller, 1972, Remote mapping of standing crop biomass for estimation of the productivity of the shortgrass prairie, Pawnee National Grasslands, Colorado. Proceedings of the 8th International Symposium on Remote Sensing of the Environment, II: 1355-1379.

Kokaly, R., 2000, Investigating a physical basis for spectroscopic estimates of leaf nitrogen concentration. Remote Sens. Environ. (in press).

Maas, S. and J. Dunlap, 1989, Reflectance, absorptance, and transmittance of light by normal, etiolated, and albino corn leaves. Agron. J., 81: 105-110.

Papoulis, A., 1965, Probability, Random Variables, and Stochastic Processes. New York: McGraw-Hill.

Rouse, J., 1973, Monitoring the vernal advancement and retrogradation of natural vegetation. NASA Report, Greenbelt, MD.

Rundquist, D. and L. Di, 1989, Band moment analysis of imaging spectrometer data. Photogramm. Eng. Rem. S., 55: 203-208.

Schepers, J., T. Blackmer, W. Wilhelm, and M. Resende, 1996, Transmittance and reflectance measurements of corn leaves from plants with different nitrogen and water supply. J. Plant Physiol., 148: 523-529.

Semenov, A. and V. Yefremenko, 1999, Algorithms for processing multispectral images with certain invariant properties. Mapping Sciences and Remote Sensing, 36: 125-132.

Siegel, S., 1956, Non-parametric Statistics. McGraw-Hill, New York.

Staenz, K., 1996, Classification of a hyperspectral agricultural data set using band moments for reduction of the spectral dimensionality. Canadian Journal Rem. Sens., 22: 248-257.

Thenkabail, P., R. Smith, and E. De Pauw, 2000, Hyperspectral vegetation indices and their relationships with agricultural crop characteristics. Rem. Sens. Environ., 71: 158-182.

Thomas, I., N. Ching, V. Benning, and J. D'Aguanno, 1987, A review of multi-channel indices of class separability. Int. J. Remote Sens., 8: 331-350.

Woolley, J., 1971, Reflectance and transmittance of light by leaves. J. Plant Physiol., 47: 656-662.